Anomalous Nernst effect in perovskite La$_{0.5}$Ca$_{0.5}$CoO$_3$

A. Ghosh, M. Manikandan, and R. Mahendiran

Department of Physics, National University of Singapore, 2 Science Drive 3, Singapore 117551, Republic of Singapore

We report the occurrence of the anomalous Nernst effect (ANE) in polycrystalline perovskite La$_{0.5}$Ca$_{0.5}$CoO$_3$. The sample is ferromagnetic below T_C = 147 K and resistivity shows non-metallic behavior above and below the T_C with only a small negative magnetoresistance (~2%) around T_C. Field dependence of magnetization at 10 K shows large hysteresis with a coercive field of 6 kOe but a small magnetization ~ 0.64 μ_B/Co even in a field of 50 kOe, which indicates the presence of magnetically heterogeneous ground state consisting of ferromagnetic and non-ferromagnetic phases. The field dependence of the Nernst thermopower (S_{xy}) at low temperatures shows complete saturation but the magnetization does not. This indicates that the ANE in La$_{0.5}$Ca$_{0.5}$CoO$_3$ depends only on the transport properties of the ferromagnetic phase, while it is not affected by the non-ferromagnetic phase. Due to the higher value of remnant S_{xy}, the magnetized polycrystalline sample exhibits ANE in absence of an external magnetic field.

Index Terms— **Anomalous Nernst effect, Perovskite Oxide, Spincaloritronics.**

I. INTRODUCTION

THE conversion of heat into spin-dependent electrical signals (spincaloritronics) has drawn immense attention in the last decade to find better, faster and energy saving technologies [1]–[6]. In this aspect, phenomena like, spin Seebeck effect (SSE) [5], anomalous Nernst effect (ANE) [3] and spin Nernst effect (SNE) [6] are being studied. The ANE has become very popular for its comparatively larger efficiency in converting heat into spintronic signal and simplicity in device fabrication [3], [4]. The Nernst effect is measured as the electric field developed in a material in *y*-direction due to the Lorentz force and/or spin-orbit coupling (SOC) experienced because of the mutual effects of thermal gradient (∇T) and magnetic field (H) applied independently in the *x* and *z*-directions. The ordinary Nernst effect (NE) arises due the Lorentz force experienced by the conduction electrons of a material and thus it is proportional to the applied magnetic field. The ANE is deeply connected to SOC and its magnetic field dependence at a fixed temperature usually follows the magnetization curve of a material. However, the magnitude of the ANE thermopower has no correlation with the saturation magnetization [7]–[9].

To date, several metals, alloys and oxide materials have been investigated to understand the origin of ANE and to find ways to enhance its magnitude for better application possibilities. In addition to soft ferromagnets (Co, Ni, Fe and their alloys [2], [10]), ANE was also reported in hard ferromagnet such as SmCo$_5$ [11] and topological ferromagnets such as Co$_2$MnGa [12], Co$_3$Sn$_2$S$_2$ [13], Nd$_2$Mo$_2$O$_7$ [14], etc. While Co$_2$MnGa shows the highest anomalous Nernst thermopower (S_{xy}^{ANE}) around room temperature (~ 6 μV/K) [12], SmCo$_5$ exhibits the largest anomalous transverse thermoelectric conductivity (α_{xy}^{ANE}) at room temperature (~ 4.6 A/K m) [11]. ANE is expected to be negligible in antiferromagnets. However, some antiferromagnets with non-colinear spin structure such as Mn$_3$Sn [15], [16], YbMnBi$_2$ [17], CoNb$_3$S$_6$ [18], shows an unusually high value of ANE that does not scale with magnetization. The α_{xy}^{ANE} in YbMnBi$_2$ reaches ~ 10 μV/K m for YbMnBi$_2$ below 100 K, which is the largest value reported to date [17]. It is believed that Berry curvature of the conduction

band near the Fermi level in these materials acts as fictious magnetic field to asymmetrically scatter spin up and spin down charge carries leading to the large ANE values. In this context, ANE in oxide materials are relatively less explored. La$_{0.7}$Sr$_{0.3}$CoO$_3$ [2], [19], Pr$_{0.5}$Sr$_{0.5}$CoO$_3$ [20], R$_{0.6}$Sr$_{0.4}$CoO$_3$ (R = La, Pr, Nd) [21] and Fe$_3$O$_4$ [1] are few of these oxides that have shown their potential for ANE in both the single and polycrystalline phases.

While LaCoO$_3$ is a non-magnetic insulator, divalent alkaline earth cation (Sr^{2+}, Ca^{2+}, Ba^{2+}) substitution for the La^{3+} rare-earth ion brings in ferromagnetism and metallic conduction. The divalent cation substitution not only partially transforms Co^{3+} into Co^{4+}, but also transforms the spin state. While Co^{3+} ion is primarily in low spin state (t$_{2g}^6$e$_g^0$) in LaCoO$_3$, it is transformed into intermediate spin state (t$_{2g}^5$e$_g^1$) in the doped compounds. It is believed that ferromagnetism in these oxides is due to double exchange interaction between intermediate spins Co^{3+} (t$_{2g}^5$e$_g^1$) and low spins Co^{4+} (t$_{2g}^5$e$_g^0$) ions [22]. La$_{0.5}$Ca$_{0.5}$CoO$_3$ possesses an orthorhombic (space group: *Pnma*) structure and shows a ferromagnetic (FM) ordering near 150 K [23]. It was suggested that the low temperature phase may be heterogeneous in which the non-percolating FM phase may coexist with the non-FM phase [24], [25], and thus it may be interesting to study the ANE. In this work, we studied the ANE in polycrystalline La$_{0.5}$Ca$_{0.5}$CoO$_3$ and found that the ANE is mainly sensitive to the FM part of the sample and thus, does not follow the non-saturating magnetization as observed due to the alignment of the non-FM phase at low temperatures. The sample also exhibited zero-field ANE in the magnetized state.

II. EXPERIMENTAL

Polycrystalline La$_{0.7}$Ca$_{0.3}$CoO$_3$ was synthesized by the solid-state reaction from stoichiometrically mixed pre-heated powders of La$_2$O$_3$, CaCO$_3$, and Co$_3$O$_4$. After consecutive grinding and heating of the powder several times at 1000°C and 1100° C for 12 hours, the powder was finally pressed into pellets and sintered at 1200°C for 24 hours in the air. Magnetic measurements were carried out in a vibrating sample magnetometer (VSM) attached to the physical property measurement system (PPMS). Resistivity and longitudinal
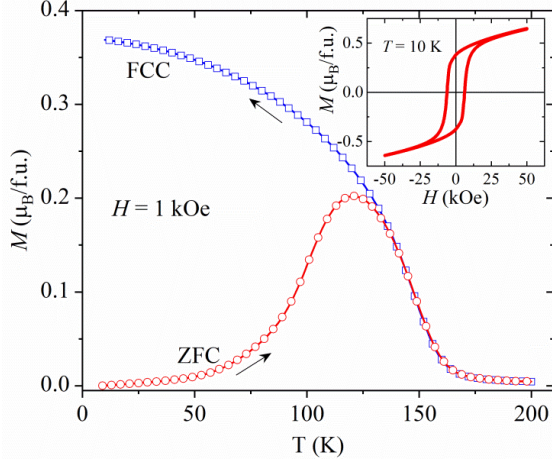
Fig. 1. Zero field cooled (ZFC) and field cooled cooling (FCC) temperature dependence of the magnetization at $H = 1$ kOe. Inset: Field dependence of the magnetization measured at $T = 10$ K.

thermopower were simultaneously measured in a homemade probe attached to the PPMS. For ANE measurement, a rectangular-shaped sample of typical dimension $\sim 5 \times 3 \times 0.5$ mm^3 was cut and polished. The ANE was measured in a custom designed homemade probe attached to the PPMS which is discussed in detail in our earlier work [20]. In this setup, the sample is placed between the top of two copper blocks maintained at two different temperatures creating an in-plane temperature difference (ΔT). The bottom and top surfaces of the sample may have different temperatures depending on the thermal conductivity of the measured sample and thus it can create an error in measuring the actual value of ΔT [26]. This can underestimate the obtained value of Nernst thermopower (S_{xy}) by 5-10% for the sample reported here. The S_{xy} was measured as a function of applied magnetic field (H), and the voltages generated from longitudinal thermopowers of the sample and measurement leads were subtracted as, $S_{xy} = \frac{1}{2} \frac{\left(V_{xy}(+H) - V_{xy}(-H) \right)/l_y}{\Delta T_x / l_x}$ where l_y is the distance between the measurement leads along y-direction and l_x is the distance between the two copper blocks along the x-direction (a schematic is given in Fig. 3(d) showing the measurement configuration).

III.   RESULT AND DISCUSSION

A. Magnetic Properties

Fig. 1 shows the temperature dependence of zero-field cooled (ZFC) and field cooled cooling (FCC) magnetization for La$_{0.5}$Ca$_{0.5}$CoO$_3$ measured in the presence of $H = 1$ kOe magnetic field. ZFC magnetization increases with temperature, exhibit a maximum near 120 K and decreases rapidly across the Currie temperature (T_C) $\sim$ 147 K. The FCC curve follows the ZFC magnetization near the T_C, bifurcate near 120 K and increase monotonically with decreasing the temperature. Such irreversibility in magnetization may arise due to the breakdown of long-range ferromagnetic order and emergence of cluster spin-glass state or freezing of magnetic domains in random directions in the ZFC mode if the measuring field is much lower

than the anisotropy field [27], [28]. The field dependence of magnetization (*M-H* curve) at 10 K plotted in the inset of Fig. 1 exhibits hysteresis with a large coercive field, $H_C \sim$ 6 kOe. The *M-H* curve at 10 K (as shown in the inset) does not show saturation up to 50 kOe, where M reaches 0.65 μ_B/Co, a value much less than 1.62 μ_B/Co found in La$_{0.5}$Sr$_{0.5}$CoO$_3$ [22]. However, the observed value of magnetization in our composition is closer to 0.61 μ_B/Co at 10 K as obtained by neutron diffraction study of La$_{0.9}$Ca$_{0.1}$CoO$_3$ sample, in which long range ferromagnetism was already found [29]. It is likely that the FM phase coexists with the non-FM phase in our sample. While Co^{3+}/Co^{4+} ions are in intermediate spin / low-spin configurations mediating FM interaction in the FM phase, Co^{3+} ions are in low-spin state (S = 0) in the non-FM phase. However, we are not discussing this aspect in detail as the scope of this paper is restricted to study the ANE.

B. Longitudinal Resistivity and Thermopower

Fig. 2(a) shows the temperature dependence of the longitudinal resistivity (ρ_{xx}) measured at $H = 0$ and 50 kOe fields. The sample exhibits non-metallic resistivity where the value of ρ_{xx} increases more than 100 times from 250 K to 10 K. As the magnetic field has an insignificant effect on the resistivity in the scale of the temperature dependent plots, we measured the field sweep in the vicinity of T_C and obtained $\sim$ -2% magnetoresistance (MR) at 150 K as shown in the inset of Fig. 2(a). The MR was calculated as the percentage change in ρ_{xx} under the magnetic field which can be expressed as, $MR = \frac{(\rho_{xx}^H - \rho_{xx}^0)}{\rho_{xx}^0} \times 100\%$ where ρ_{xx}^0 and ρ_{xx}^H are respectively the resistivity values in the absence and presence of an external magnetic field.

The temperature dependence of the longitudinal thermopower (S_{xx}) is plotted in Fig. 2(b) for the same fields as the resistivity. The positive sign of S_{xx} indicates holes as the majority carrier. S_{xx} shows a clear change in slope near the T_C and continuously decreases at low temperatures. The change in slope of S_{xx} around T_C implies a decrease in scattering felt by charge carriers diffusing under the temperature gradient due to spin alignment, *i.e.*, decrease in spin-disorder scattering. The value of thermopower decreases in the presence of $H = 50$ kOe in a narrow temperature region around T_C, whereas both the curves merge far below and above T_C. Application of the magnetic field enhances the spin alignment and thus reduces spin-disorder scattering near T_C which leads to a longer mean free path for the heat carrying charges as compared to the zero field case. Since spin-disorder scattering is negligible even in zero field at temperatures much below T_C, the applied magnetic field has little or no influence on the value of thermopower as seen previously in other oxides [30], [31]. The magnetothermopower (MTEP) was estimated as the percentage change in S_{xx} due to the presence of a magnetic field $\left(MTEP = \frac{(S_{xx}^H - S_{xx}^{H=0})}{S_{xx}^{H=0}} \times 100\% \right)$, where $S_{xx}^{H=0}$ and S_{xx}^H are the values of the longitudinal thermopower respectively in the absence and presence of an external magnetic field. At 150 K, a maximum MTEP of -7 % is obtained due to $H = 50$ kO (Inset of Fig. 2(b)). While the thermopower is sensitive to dynamics of charges
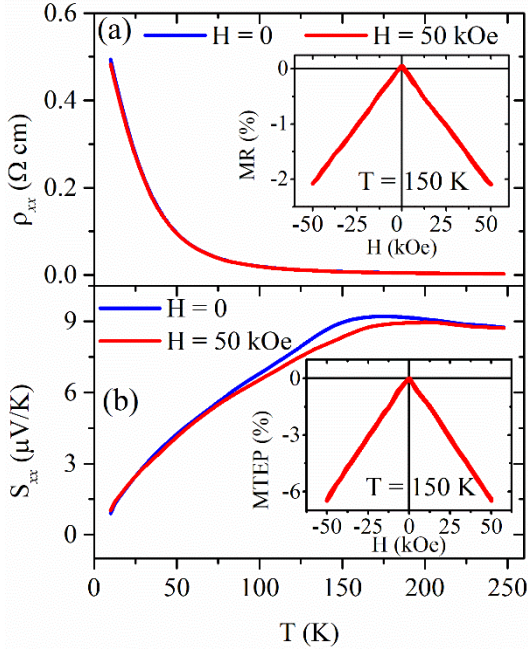
Fig. 2. (a) Temperature dependence of the longitudinal resistivity (ρ_{xx}) measured at H = 0 and 50 kOe. Inset: Field dependence of the magnetoresistance (MR) measured at 150 K. (b) Temperature dependence of the longitudinal thermopower (S_{xx}) measured at H = 0 and 50 kOe. Inset: Field dependence of the magnetothermopower (MTEP) measured at 150 K.
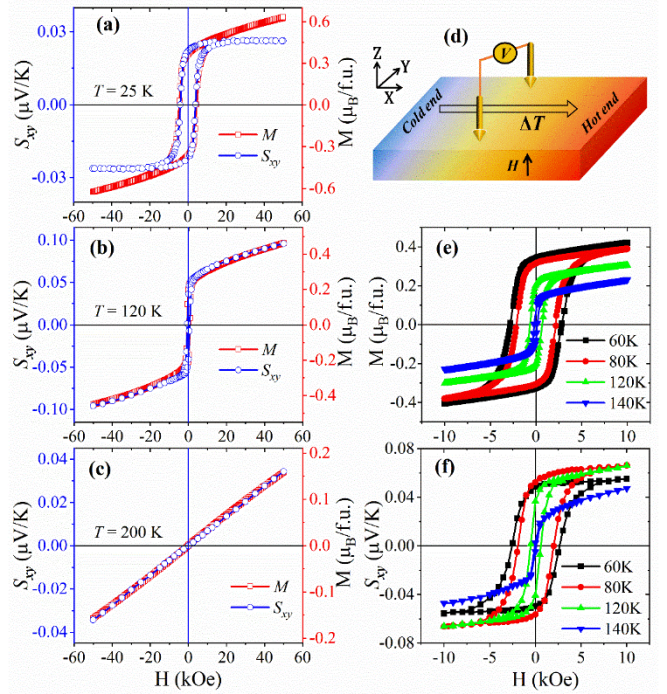

Fig. 3. Field dependences of magnetization (right vertical axis) and Nernst thermopower, S_{xy} (left vertical axis) measured at (a) T = 25 K, (b) T = 120 K and (c) T = 200 K. (d) Schematic representation of the measurement configuration for the Nernst effect. Expanded view of the low field (-10 kOe $\leq H \leq$ 10 kOe) dependence of (e) magnetization and (f) S_{xy} measured at T = 60, 80, 120 and 140 K.

within grains, the electrical resistivity is affected by both grain and grain boundary resistances. In magnetic samples, it causes semiconducting like resistivity across ferromagnetic transition, but the thermopower is found to show a prominent anomaly only around the T_C [32].

C. Field Dependence of Magnetization and Anomalous Nernst Effect

Fig. 3(d) shows schematic diagram of the measurement configuration indicating the direction of applied ΔT along x, magnetic field along z and measured voltage along y-directions Fig. 3(a) – 3(c) show the M-H curves (right vertical axis) and field dependences of the S_{xy} (left vertical axis) measured at 25, 120 and 200 K. Although, both $M(H)$ and $S_{xy}(H)$ show similar hysteresis, the data at 25 K indicates that while M does not show saturation in the maximum available field, S_{xy} saturates above H = 20 kOe. This indicates that the ANE in this material does not follow the total magnetization at 25 K. The total magnetization can be considered as the sum of the contributions coming from the FM and the non-FM phases. In this case, the nature of the S_{xy} vs H curve follows only the FM part and this implies that the non-FM contribution present in the sample does not contribute to the Nernst effect. However, S_{xy} vs H at 120 K shows non-saturating behavior and overlaps with the M vs H curve (Fig. 3(b)). At 200 K (Fig. 3(c)), both S_{xy} and M increase linearly with the magnetic field as only the normal Nernst effect is active in the paramagnetic state. Figs. 3(e) and (f) respectively show the M-H and S_{xy}-H curves measured at T = 60, 80, 120 and 140 K in the low-field regime (-10 kOe $\leq H \leq$ +10 kOe) for clarity. Both the magnetization and S_{xy} trace similar hysteresis loops with large H_C. The hysteresis becomes narrow with increasing temperature. The remnant value of S_{xy}

is significant in this material due to the larger value of H_C which gives rise to the zero-field ANE discussed later in this paper.

D. Temperature Dependence of Anomalous Nernst Effect

The high field region (H = 30-50 kOe) of the S_{xy} vs H curves was fitted linearly to extract the value of S_{xy} due to NE (S_{xy}^{NE}) and ANE (S_{xy}^{ANE}) obtained at different temperatures [19]. S_{xy}^{NE} was obtained from the slope of the linear fit as; $S_{xy}^{NE}(H) = S_{xy}^{Slope}H$ and, the anomalous contribution was extracted as; $S_{xy}^{ANE}(H) = S_{xy}(H) - S_{xy}^{NE}(H)$. The extracted S_{xy}^{ANE} is plotted as a function of temperature in Fig. 4(a) for H = 5, 10 and 50 kOe. As the temperature decreases below 180 K, S_{xy}^{ANE} increases rapidly due to magnetic ordering across the T_C, goes through a maximum near 100 K, and decreases monotonically towards zero at low temperatures. Although the S_{xy}^{ANE} vs T curves for H = 10 and 50 kOe show a similar behavior at low temperatures, the same for H = 5 kOe decreases much rapidly due to non-saturation of the sample because of the increased H_C. In addition to that, the zero-field S_{xy}^{ANE} is also plotted in the same figure (star symbol) which is same as the remnant value of S_{xy} and obtained from the S_{xy} vs H curves at H = 0 while reducing the field from 50 kOe. It is interesting to note that even at T = 120 K, an adequate value of zero-field ANE signal is obtainable. This indicates that ANE in $La_{0.5}Ca_{0.5}CoO_3$ can be obtained by applying ΔT in the absence of H if the sample is already magnetized.

Fig. 4(b) represents the temperature dependence of the anomalous transverse thermoelectric conductivity which can be expressed as [14],
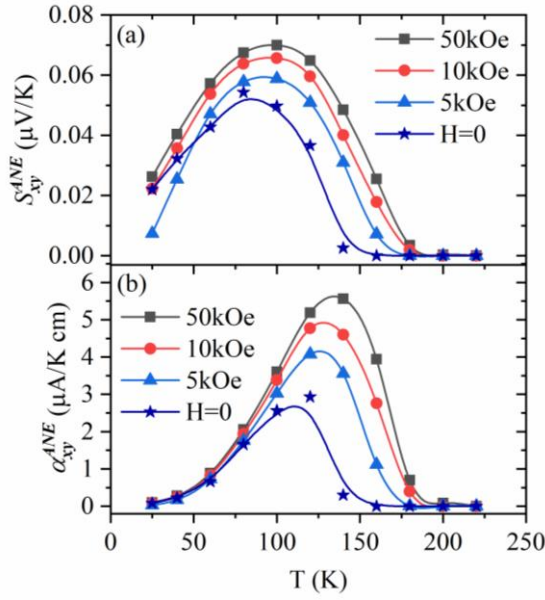
Fig. 4. Temperature dependence of the (a) anomalous Nernst thermopower (S_{xy}^{ANE}) and (b) anomalous transverse thermoelectric conductivity ($\alpha_{xy}^{ANE} \approx S_{xy}^{ANE}/\rho_{xx}$) obtained for $H = 0, 5, 10$ and 50 kOe fields. S_{xy}^{ANE} and α_{xy}^{ANE} at $H = 0$ represent the remnant values recorded after reducing the field to 0 from 50 kOe. Data points are connected through spline fitting to guide the eye.

$$\alpha_{xy}^{ANE} = [S_{xy}^{ANE} - S_{xx}(\rho_{xy}/\rho_{xx})]/\rho_{xx} \qquad (1)$$

where ρ_{xy} is the Hall resistivity. The reported value of the Hall angle, $\theta_H \approx \rho_{xy}/\rho_{xx}$ is $\sim 6.5 \times 10^{-5}$ at 100 K for La$_{0.85}$Ca$_{0.15}$CoO$_3$ single crystal [33]. This makes the second term of Eq. (1) negligible. Thus, for the samples with very low θ_H, Eq. (1) can be simplified to $\alpha_{xy}^{ANE} \approx S_{xy}^{ANE}/\rho_{xx}$. The α_{xy}^{ANE} increases rapidly across the ferromagnetic ordering temperature, goes through a peak, and rapidly decreases towards zero on the low temperature side. In metallic systems, the α_{xy}^{ANE} follows a T-linear behavior at low temperatures obeying the Mott's rule [34], but a clear deviation from the linear behavior is observed in the present compound. The resistivity of the sample increases from ~ 0.02 Ω cm at 100 K to ~ 0.3 Ω cm at 25 K which in turn drastically diminishes the value of α_{xy}^{ANE} and thus such anomaly is observed.

IV. CONCLUSION

In summary, we have studied the field and temperature dependence of the anomalous Nernst effect (ANE) in La$_{0.5}$Ca$_{0.5}$CoO$_3$. The ANE shows an abrupt increase near the ferromagnetic ordering, goes through a peak, and decreases to zero at low temperatures. While the ANE signal shows saturation at low temperatures, magnetization does not saturate. An interesting feature of this compound is the non-zero ANE value in zero magnetic field at cryogenic temperatures which might be useful for heat into spin-dependent thermoelectric conversion. Future work needs to address the magnetic ground state of La$_{0.5}$Ca$_{0.5}$CoO$_3$ by neutron diffraction and dynamic magnetic susceptibility.

ACKNOWLEDGMENT

REFERENCES

[1] R. Ramos, M. H. Aguirre, A. Anadon, J. Blasco, I. Lucas, K. Uchida, P. A. Algarabel, L. Morellon, E. Saitoh, and M. R. Ibarra, "Anomalous Nernst effect of Fe$_3$O$_4$ single crystal," *Phys. Rev. B*, vol. 90, p. 054422, 2014.

[2] T. Miyasato, N. Abe, T. Fujii, A. Asamitsu, S. Onoda, Y. Onose, N. Nagaosa, and Y. Tokura, "Crossover Behavior of the Anomalous Hall Effect and Anomalous Nernst Effect in Itinerant Ferromagnets," *Phys. Rev. Lett.*, vol. 99, p. 086602, 2007.

[3] M. Mizuguchi and S. Nakatsuji, "Energy-harvesting materials based on the anomalous Nernst effect," *Sci. Technol. Adv. Mater.*, vol. 20, pp. 262–275, 2019.

[4] Y. Sakuraba, K. Hasegawa, M. Mizuguchi, T. Kubota, S. Mizukami, T. Miyazaki, and K. Takanashi, "Anomalous Nernst Effect in L1$_0$-FePt/MnGa Thermopiles for New Thermoelectric Applications," *Appl. Phys. Express*, vol. 6, p. 33003, 2013.

[5] K. Uchida, J. Xiao, H. Adachi, J. Ohe, S. Takahashi, J. Ieda, T. Ota, Y. Kajiwara, H. Umezawa, H. Kawai, G. E. W. Bauer, S. Maekawa, and E. Saitoh, "Spin Seebeck insulator," *Nat. Mater.*, vol. 9, pp. 894–897, 2010.

[6] A. Bose and A. A. Tulapurkar, "Recent advances in the spin Nernst effect," *J. Magn. Magn. Mater.*, vol. 491, p. 165526, 2019.

[7] T. C. Chuang, P. L. Su, P. H. Wu, and S. Y. Huang, "Enhancement of the anomalous Nernst effect in ferromagnetic thin films," *Phys. Rev. B*, vol. 96, p. 174406, 2017.

[8] J. Sinova, S. O. Valenzuela, J. Wunderlich, C. H. Back, and T. Jungwirth, "Spin Hall effects," *Rev. Mod. Phys.*, vol. 87, pp. 1213–1260, 2015.

[9] K. I. Uchida, W. Zhou, and Y. Sakuraba, "Transverse thermoelectric generation using magnetic materials," *Appl. Phys. Lett.*, vol. 118, p. 140504, 2021.

[10] L. Z. Yi, D. Yang, M. Liu, H. H. Fu, L. Ding, Y. Xu, B. Zhang, L. Pan, and J. Q. Xiao, "Concepts of Spin Seebeck Effect in Ferromagnetic Metals," *Adv. Funct. Mater.*, vol. 30, p. 2004024, 2020.

[11] A. Miura, H. Sepehri-Amin, K. Masuda, H. Tsuchiura, Y. Miura, R. Iguchi, Y. Sakuraba, J. Shiomi, K. Hono, and K. I. Uchida, "Observation of anomalous Ettingshausen effect and large transverse thermoelectric conductivity in permanent magnets," *Appl. Phys. Lett.*, vol. 115, p. 222403, 2019.

[12] A. Sakai, Y. P. Mizuta, A. A. Nugroho, R. Sihombing, T. Koretsune, M. T. Suzuki, N. Takemori, R. Ishii, D. Nishio-Hamane, R. Arita, P. Goswami, and S. Nakatsuji, "Giant anomalous Nernst effect and quantum-critical scaling in a ferromagnetic semimetal," *Nat. Phys.*, vol. 14, pp. 1119–1124, 2018.

[13] S. N. Guin, P. Vir, Y. Zhang, N. Kumar, S. J. Watzman, C. Fu, E. Liu, K. Manna, W. Schnelle, J. Gooth, C. Shekhar, Y. Sun, and C. Felser, "Zero-Field Nernst Effect in a Ferromagnetic Kagome-Lattice Weyl-Semimetal Co$_3$Sn$_2$S$_2$," *Adv. Mater.*, vol. 31, p. 1806622, 2019.

[14] N. Hanasaki, K. Sano, Y. Onose, T. Ohtsuka, S. Iguchi, I. Kézsmárki, S. Miyasaka, S. Onoda, N. Nagaosa, and Y. Tokura, "Anomalous Nernst effects in pyrochlore molybdates with spin chirality," *Phys. Rev. Lett.*, vol. 100, p. 106601, 2008.

[15] S. Nakatsuji, N. Kiyohara, and T. Higo, "Large anomalous Hall effect in a non-collinear antiferromagnet at room temperature," *Nature*, vol. 527, pp. 212–215, 2015.

[16] M. Ikhlas, T. Tomita, T. Koretsune, M. T. Suzuki, D. Nishio-Hamane, R. Arita, Y. Otani, and S. Nakatsuji, "Large anomalous Nernst effect at room temperature in a chiral antiferromagnet," *Nat. Phys.*, vol. 13, pp. 1085–1090, 2017.

[17] Y. Pan, C. Le, B. He, S. J. Watzman, M. Yao, J. Gooth, J. P. Heremans, Y. Sun, and C. Felser, "Giant anomalous Nernst signal in the antiferromagnet YbMnBi$_2$," *Nat. Mater.*, 2021.

[18] N. J. Ghimire, A. S. Botana, J. S. Jiang, J. Zhang, Y. S. Chen, and J. F. Mitchell, "Large anomalous Hall effect in the chiral-lattice antiferromagnet CoNb$_3$S$_6$," *Nat. Commun.*, vol. 9, p. 3280, 2018.

[19] M. Soroka, K. KníŽek, Z. Jirák, P. Levinský, M. Jarošová, J. Buršík, and J. Hejtmánek, "Anomalous Nernst effect in the ceramic and thin film samples of La$_{0.7}$Sr$_{0.3}$CoO$_3$ perovskite," *Phys. Rev. Mater.*, vol. 5, p. 035401, 2021.

[20] A. Ghosh, A. Chanda, and R. Mahendiran, "Anomalous Nernst effect in Pr$_{0.5}$Sr$_{0.5}$CoO$_3$," *AIP Adv.*, vol. 11, p. 035031, 2021.

[21] A. Ghosh, A. Chanda, M. Manikandan, and R. Mahendiran, "Rare earth

size dependence of Nernst thermopower in ferromagnetic perovskites: $R_{0.6}Sr_{0.4}CoO_3$ (R = La, Pr, and Nd)," *J. Magn. Magn. Mater.*, vol. 537, p. 168240, 2021.

[22] M. A. Señarís-Rodríguez and J. B. Goodenough, "Magnetic and transport properties of the system $La_{1-x}Sr_xCoO_{3-\delta}$ (0 < x ≤ 0.50)," *J. Solid State Chem.*, vol. 118, pp. 323–336, 1995.

[23] N. O. Golosova, D. P. Kozlenko, E. V. Lukin, and B. N. Savenko, "Effect of high pressure on the crystal and magnetic structures of $La_{0.5}Ca_{0.5}CoO_3$ cobaltite," *JETP Lett.*, vol. 92, pp. 110–114, 2010.

[24] J. C. Debnath, R. Zeng, J. H. Kim, P. Shamba, D. P. Chen, and S. X. Dou, "Effect of frozen spin on the magnetocaloric property of $La_{0.7}Ca_{0.3}CoO_3$ polycrystalline and single crystal samples," *J. Alloys Compd.*, vol. 510, p. 125, 2012.

[25] I. Fita, R. Szymczak, R. Puzniak, I. O. Troyanchuk, J. Fink-Finowicki, Y. M. Mukovskii, V. N. Varyukhin, and H. Szymczak, "Pressure-tuned spin state and ferromagnetism in $La_{1-x}M_xCoO_3$ (M=Ca,Sr)," *Phys. Rev. B*, vol. 71, p. 214404, 2005.

[26] R. Iguchi, K. I. Uchida, S. Daimon, and E. Saitoh, "Concomitant enhancement of the longitudinal spin Seebeck effect and the thermal conductivity in a Pt/YIG/Pt system at low temperatures," *Phys. Rev. B*, vol. 95, p. 174401, 2017.

[27] R. Ganguly, I. K. Gopalakrishnan, and J. V. Yakhmi, "Influence of the size of dopant ion on ferromagnetic behavior of $Ln_{0.7}A_{0.3}CoO_3$ system [Ln = La, Nd; and A = Ca, (Ca, Sr), Sr, (Sr, Ba), Ba]," *Phys. B Condens. Matter*, vol. 271, pp. 116–124, 1999.

[28] P. S. Anil Kumar, P. A. Joy, and S. K. Date, "Origin of magnetic anomalies in the spin glass system, $La_{0.85}Sr_{0.15}CoO_3$," *J. Appl. Phys.*, vol. 83, pp. 7375–7377, 1998.

[29] J. C. Burley, J. F. Mitchell, and S. Short, "Competing electronic ground states in $La_{1-x}Ca_xCoO_3$," *Phys. Rev. B*, vol. 69, p. 054401, 2004.

[30] D. V. Maheswar Repaka, T. S. Tripathi, M. Aparnadevi, and R. Mahendiran, "Magnetocaloric effect and magnetothermopower in the room temperature ferromagnet $Pr_{0.6}Sr_{0.4}MnO_3$," *J. Appl. Phys.*, vol. 112, p. 123915, 2012.

[31] P. Kumar and R. Mahendiran, "Magnetothermopower, magnetic entropy change, and magnetoresistance in ferromagnetic cobaltites: $R_{0.7}Sr_{0.3}CoO_3$ (R = La and Gd)," *Appl. Phys. Lett.*, vol. 106, p. 142401, 2015.

[32] R. Mahendiran, R. Mahesh, A. K. Raychaudhuri, and C. N. R. Rao, "Resistivity, giant magnetoresistance and thermopower in $La_{0.7}Sr_{0.3}MnO_3$ showing a large difference in temperatures corresponding to the ferromagnetic transition and the insulator - Metal transition," *Solid State Commun.*, vol. 99, pp. 149–152, 1996.

[33] S. A. Baily, M. B. Salamon, Y. Kobayashi, and K. Asai, "Anomalous Hall effect in $La_{1-x}Ca_xCoO_3$," *Appl. Phys. Lett.*, vol. 80, pp. 3138–3140, 2002.

[34] Y. Pu, D. Chiba, F. Matsukura, H. Ohno, and J. Shi, "Mott Relation for Anomalous Hall and Nernst Effects in $Ga_{1-x}Mn_xAs$ Ferromagnetic Semiconductors," *Phys. Rev. Lett.*, vol. 101, p. 117208, 2008.